EARTHQUAKE ENGINEERING AND STRUCTURAL DYNAMICS
Earthquake Engng Struct. Dyn. 2006; **35**:547–575
Published online 10 February 2006 in Wiley InterScience (www.interscience.wiley.com). DOI: 10.1002/eqe.543

The role of soil in the collapse of 18 piers of Hanshin Expressway in the Kobe earthquake

George Mylonakis[1,*,†], Costis Syngros[2], George Gazetas[3] and Takashi Tazoh[4]

[1]*Department of Civil Engineering, University of Patras, Greece*
[2]*Langan Engineering and Environmental Services, New York, U.S.A.*
[3]*National Technical University, Athens, Greece*
[4]*Institute of Technology of Shimizu Corporation, Tokyo, Japan*

SUMMARY

An investigation is presented of the collapse of a 630 m segment (Fukae section) of the elevated Hanshin Expressway during the 1995 Kobe earthquake. The earthquake has, from a geotechnical viewpoint, been associated with extensive liquefactions, lateral soil spreading, and damage to waterfront structures. Evidence is presented that soil–structure interaction (SSI) in non-liquefied ground played a *detrimental* role in the seismic performance of this major structure. The bridge consisted of single circular concrete piers monolithically connected to a concrete deck, founded on groups of 17 piles in layers of loose to dense sands and moderate to stiff clays. There were 18 spans in total, all of which suffered a spectacular pier failure and transverse overturning. Several factors associated with poor structural design have already been identified. The scope of this work is to extend the previous studies by investigating the role of soil in the collapse. The following issues are examined: (1) seismological and geotechnical information pertaining to the site; (2) free-field soil response; (3) response of foundation-superstructure system; (4) evaluation of results against earlier studies that did not consider SSI. Results indicate that the role of soil in the collapse was multiple: *First*, it modified the bedrock motion so that the frequency content of the resulting surface motion became disadvantageous for the particular structure. *Second*, the compliance of soil and foundation altered the vibrational characteristics of the bridge and moved it to a region of stronger response. *Third*, the compliance of the foundation increased the participation of the fundamental mode of the structure, inducing stronger response. It is shown that the increase in inelastic seismic demand in the piers may have exceeded 100% in comparison with piers fixed at the base. These conclusions contradict a widespread view of an always-beneficial role of seismic SSI. Copyright © 2005 John Wiley & Sons, Ltd.

KEY WORDS: bridge; pier; inelastic response; numerical analysis; piles; soil–structure interaction

*Correspondence to: George Mylonakis, Department of Civil Engineering, University of Patras, GR-26500, Greece.
†E-mail: mylo@upatras.gr

Contract/grant sponsor: National Science Foundation U.S.–Japan Collaborative Program; contract/grant number: NSF 0000101
Contract/grant sponsor: University of Patras; contract/grant number: B.388

Received 13 October 2004
Revised 23 August 2005
Accepted 23 August 2005

INTRODUCTION

In the devastation caused by Kobe earthquake [1–7], the collapse and transverse overturning of the 630 m section of Hanshin Expressway at Fukae was perhaps the most spectacular failure and became the 'trademark' of the disaster in the press. The collapsed bridge section was part of elevated Route 3 that runs parallel to the shoreline. Completed in 1969, the concrete deck was connected monolithically to reinforced concrete piers, with circular cross-sections of 3.1–3.3 m in diameter and approximately 12 m in height. The typical pier was anchored inside an embedded pile-cap, on top of a group of 16–17 end-bearing piles. The main characteristics of a typical pier are depicted in Figures 1 and 2.

Detailed investigations of the seismic performance of the superstructure are available [8–14]. In these studies, several factors associated with poor structural design have been identified.

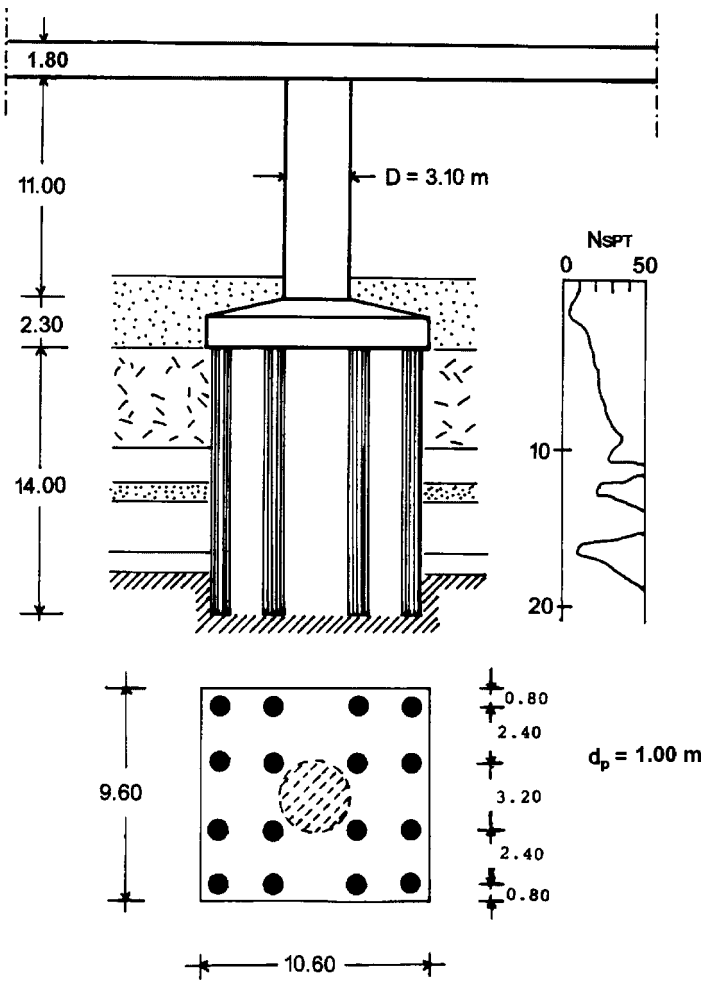

Figure 1. Geometric characteristics of a typical collapsed pier in Fukae section.

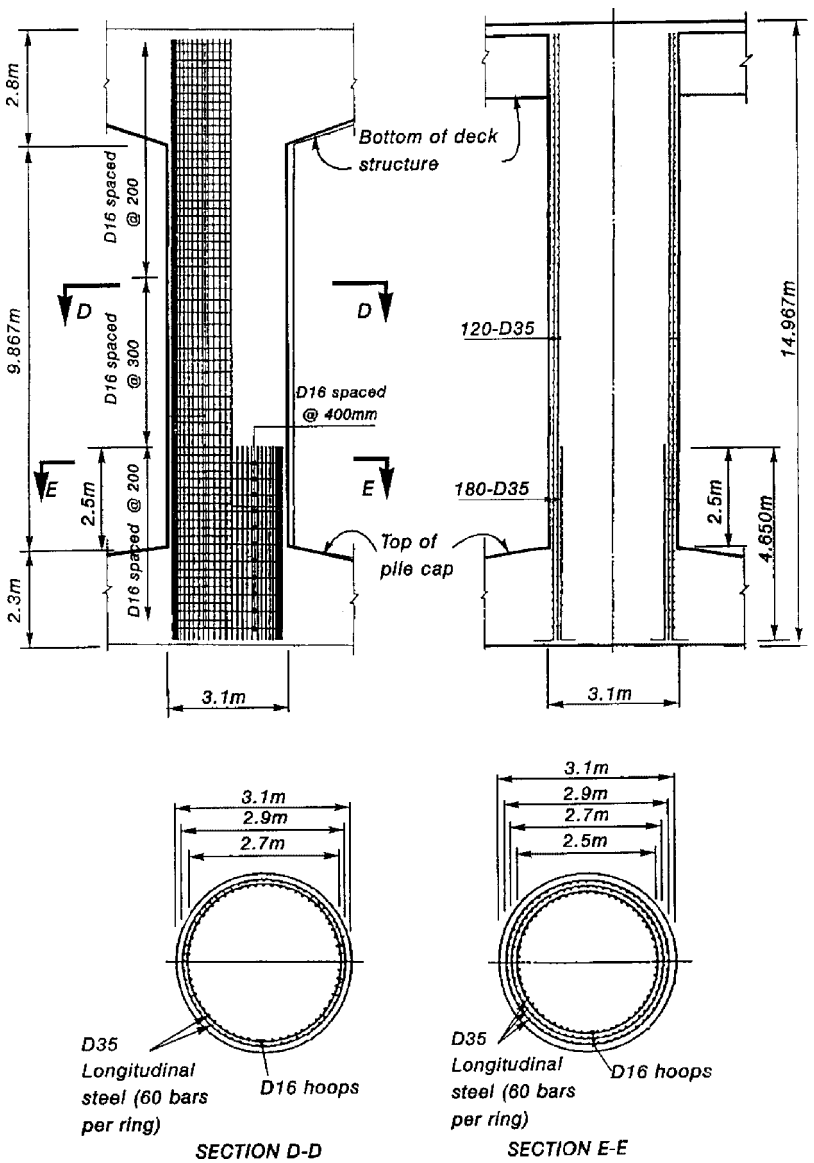

Figure 2. Pier reinforcement and structural details (after Iwasaki *et al.* [7]).

These include: (1) inadequate transverse reinforcement in the piers; (2) poor anchorage of longitudinal reinforcement; (3) use of non-conservative (elastic) methods for determining design shear forces. Notwithstanding the importance of these findings, there is evidence presented in this paper, that local soil conditions and dynamic interaction between foundation and superstructure further aggravated its inelastic behaviour, thereby contributing to the collapse.

An additional concern comes from the fact that soil–structure interaction (SSI) has been traditionally considered as *beneficial* for seismic response. Apparently, this perception stems from oversimplifications in the nature of seismic demand adopted in seismic code provisions. The most important of these simplifications (with reference to SSI) are [15]: (1) design acceleration spectra that decrease monotonically with increasing structural period; (2) response modification coefficients (i.e. 'behaviour' factors used to derive seismic forces) which are either period independent, or increase with increasing structural period; (3) foundation damping derived assuming homogeneous halfspace conditions for the soil, which tends to over predict overall effective damping [16, 17]; (4) kinematic response coefficients for spread footings indicating that foundation response is smaller than the free-field soil motion [18, 19]. The above perception is reinforced by the lack of a sufficient number of structural failures associated with SSI.

This apparently beneficial role of SSI, although realistic in many cases, has essentially turned into a dogma. Although some detrimental effects of SSI have been pointed out in the past (e.g. References [15, 16, 20–24]) and have been incorporated into modern seismic provisions [25], designers usually avoid the complication of accounting for SSI, as a conservative simplification that supposedly leads to improved safety margins.

The work reported in this paper involves: (1) discussion of seismological and geotechnical information pertaining to the bridge site; (2) analysis of free-field response; (3) dynamic response analysis of the foundation-superstructure system; (4) evaluation of results through comparisons with earlier studies that did not consider SSI.

THE FIRST ROLE OF SOIL: INFLUENCE ON GROUND MOTIONS

Kobe and the nearby towns of Asiya, Nisinomiya, and Amagasaki are built along the shoreline in the form of an elongated rectangle with length of about 30 km and width 2–3 km. The granitic bedrock that outcrops in the mountain region bordering the city to the north, dips steeply in the northwest–southwest region; in the shoreline it lies at a depth of about 1–1.5 km [7, 26, 27]. Figures 3(a) and (b) show an approximate geologic plan and a cross-section of the region including the locations of strong motion accelerometers.

The main shock was recorded in several strong motion instruments. A number of these recordings were of unusually high intensity, with peak ground accelerations (PGAs) and peak ground velocities (PGVs) in excess of $0.8g$ and 100 cm/s, respectively. PGAs in non-liquefied ground were over $0.5g$ throughout Kobe, Asiya, and Nishinomiya. PGAs above $0.4g$ were recorded at 17 sites, while at least in three locations ('JMA', 'Fukiai', and 'Motoyama') they reached the astounding $0.80g$. A comprehensive motion catalog of the Kobe earthquake has been published by Fukushima *et al.* [29].

Variability in local soil conditions among the recording stations might be partly responsible for the significant differences in intensity and frequency content of the recordings, as clearly shown in Figures 4 and 5. Three additional effects, however, seem to have affected the surface motions in the meizoseismal region: *forward rupture directivity*, *basin effects*, and *soil liquefaction*.

The first is of a seismological nature, affecting ground shaking at near-fault sites located in the direction of fault rupture propagation [30, 31]. The effect of forward fault-rupture directivity in strike-slip faulting is primarily to increase the intensity of the horizontal component of

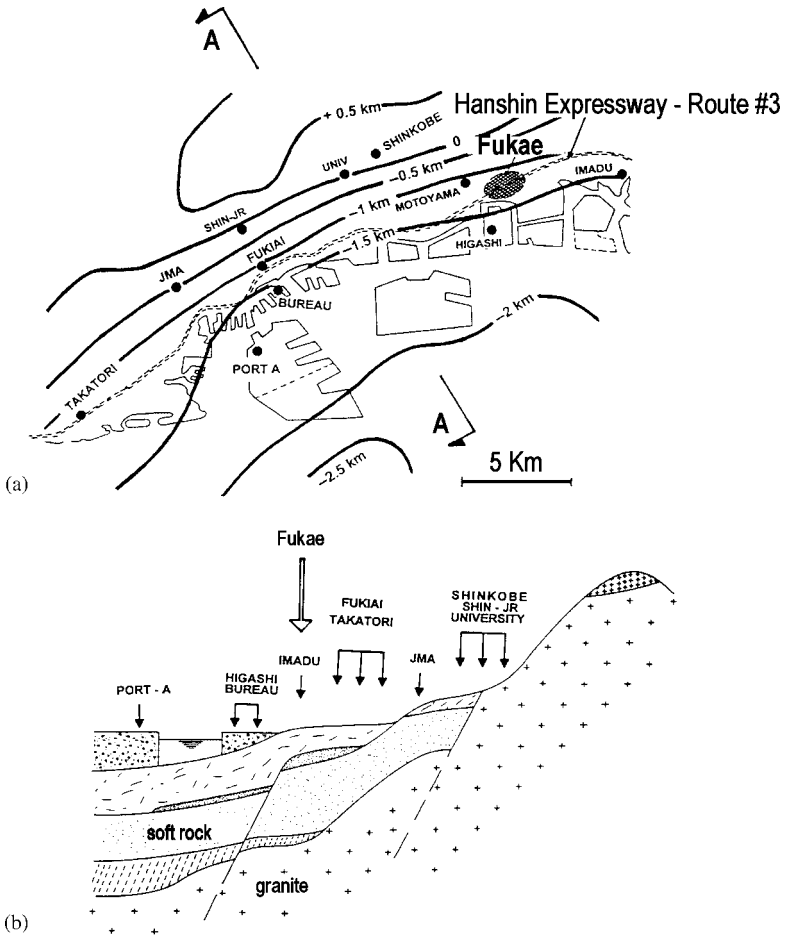

Figure 3. (a) Contours of bedrock elevation and location of accelerometers; and (b) approximate geologic section A-A (after Gazetas [28]).

the motion *normal* to the fault strike, at periods longer than about 0.5 s. The resulting differences between fault-normal (FN) and fault-parallel (FP) components in the response spectra (Figure 6) are indeed striking.

The 2D basin (valley) effect has been shown to increase or decrease the intensity, duration, and frequency characteristics of ground motion depending on the proximity to the edge of the valley, the dipping angle, the frequency content of the excitation, and the incidence wave angles [26]. Finally, soil liquefaction often results in reduction of high-frequency acceleration peaks, increase of dominant periods of vibration and in large permanent deformations if static (permanent) shear stresses exist in the ground. Liquefaction effects were highly pronounced in the near shore region during this event [5, 32].

Additional evidence on source directivity is given in Figure 7: *polar plots* of spectral accelerations in horizontal plane are presented for four acceleration records and three selected

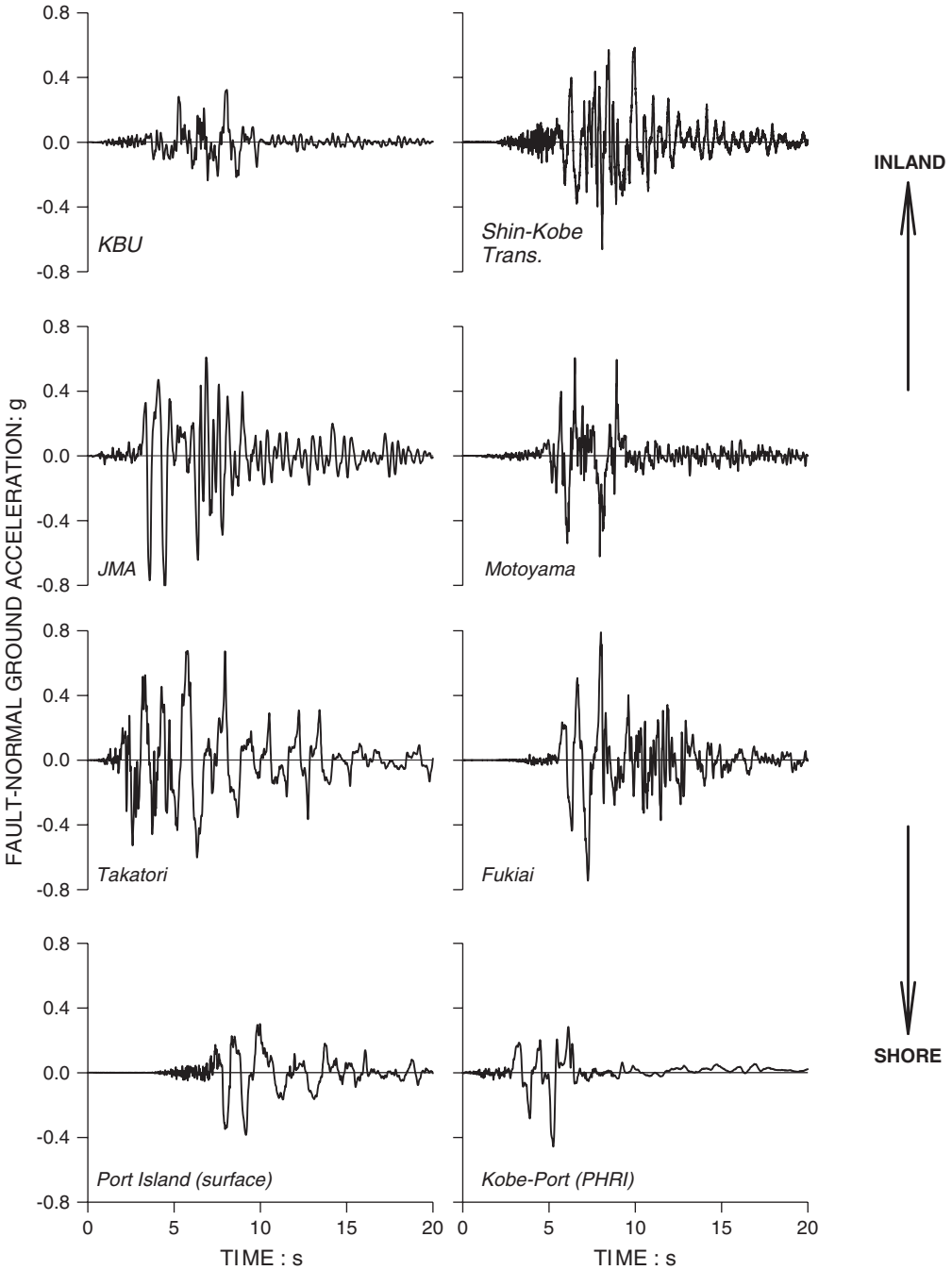

Figure 4. Selected accelerograms from Kobe earthquake. All time histories are oriented normal to fault (E127N).

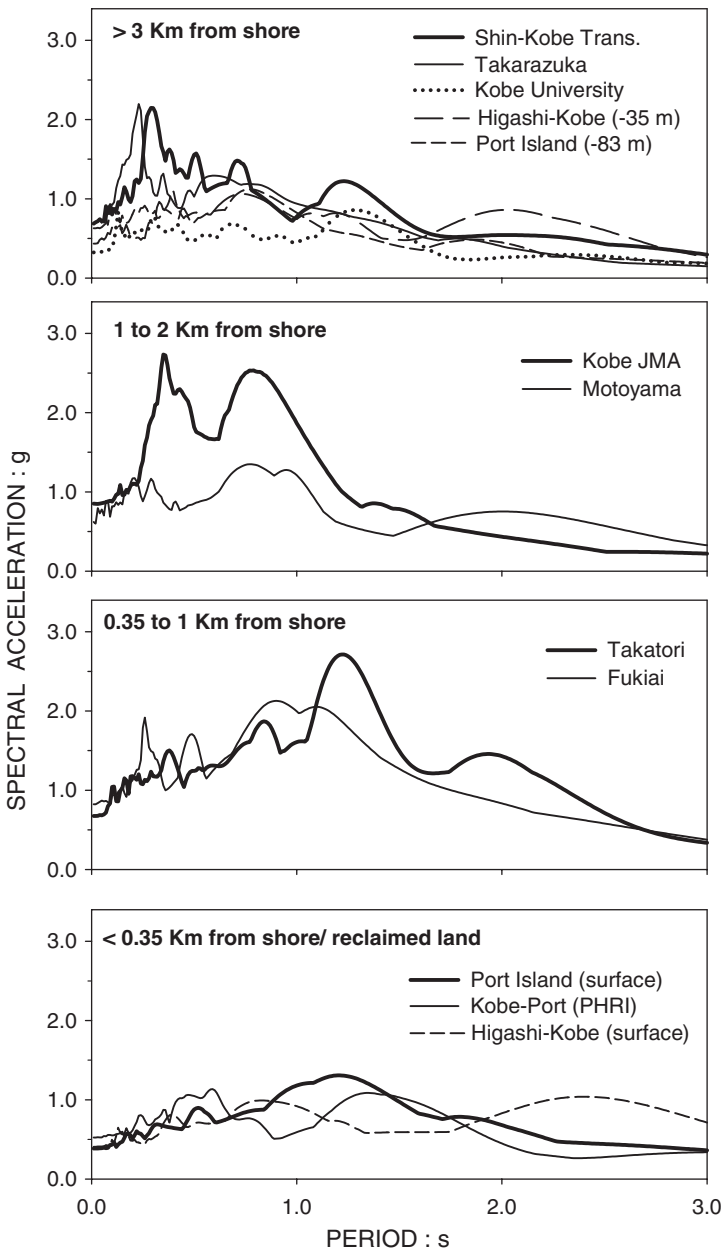

Figure 5. Fault-normal acceleration spectra with respect to distance from shore. Note the difference in predominant periods among the various groups; $\zeta = 5\%$.

periods. The fault-normal and fault-parallel directions are indicated in the graphs. It is evident that long-period acceleration components ($T > 0.6$ s) attain their maxima in the fault-normal direction and their minima in the fault-parallel direction. The opposite seems to be true with

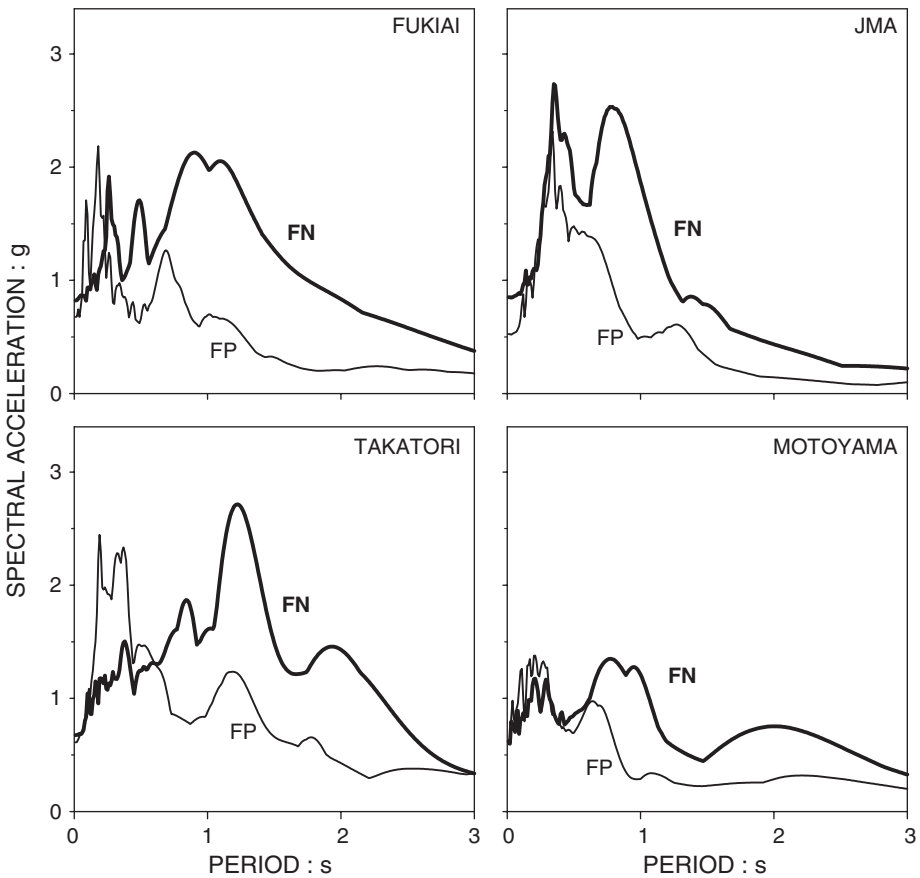

Figure 6. Elastic response spectra of selected records at fault-normal (FN) and fault-parallel (FP) orientations; $\zeta = 5\%$.

short-period components (with the exception of JMA record). In contrast, PGA is essentially independent of azimuth. Note that these attributes seem to be independent of local soil conditions, as evident from the 'Port Island' record [6].

All these effects have contributed more or less to the differences in ground motions observed in Figure 5. Evidently, the closer the site to the shore, the deeper and softer the soil deposit, thereby leading to a longer predominant period and a flatter spectrum. Interestingly, site groups in Figure 5 differ not only with respect to distance from shore, and stiffness, but also with respect to distance from fault (recall that fault trace is essentially parallel to the shoreline).

Ground shaking at the site

Unfortunately, no records were obtained close to the bridge site during the main shock. The closest stations were Motoyama and Higashi (see Figure 3), located at distances of about 1 km from the site.

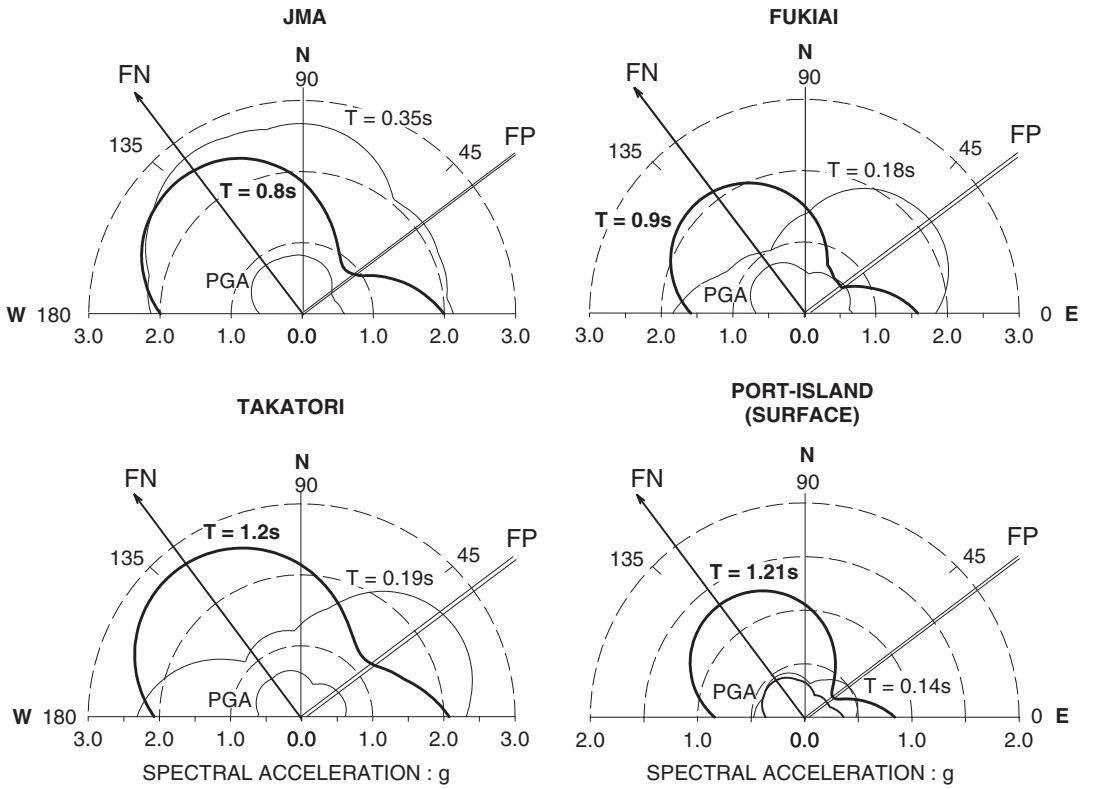

Figure 7. Polar plots of spectral accelerations for four selected records. Shown periods correspond to peak spectral values in the short and long period range. Note the pronounced values in the fault-normal (FN) direction at long periods; $\zeta = 5\%$.

From available borehole data (Figures 8 and 9), the soil at the site (Pier 138) is deemed a relatively deep deposit of moderately dense to loose layers of sand and gravel and soft to stiff clay layers with low-strain shear-wave velocity ($V_{s,\max}$) of the order of 200–300 m/s for the upper 20 m. No significant permanent deformations or evidence of liquefaction were observed after the earthquake.

Six acceleration records, all of them recorded on different soil conditions and with different frequency characteristics are used in the response analysis of the bridge piers. These are the 'Fukiai', 'Takatori', 'JMA', 'Motoyama', 'Higashi' and a synthetic accelerogram referred to as 'Synthetic'. An overview of local soil conditions and motion parameters for each motion is given in Table I.

Of the above records, Fukiai and Takatori, although recorded far from the bridge (Figure 3), are believed to be the most representative of the motion at the site, because: (a) of their similar distance from fault and shoreline; (b) of the similar orientation with respect to rupture as the collapsed segment; (c) of the similar soil conditions. The third accelerogram, JMA, was selected because it has been invariably used (often as the only record) in previous studies of the collapse (e.g. References [9, 10]). It was obtained much closer to fault and on much

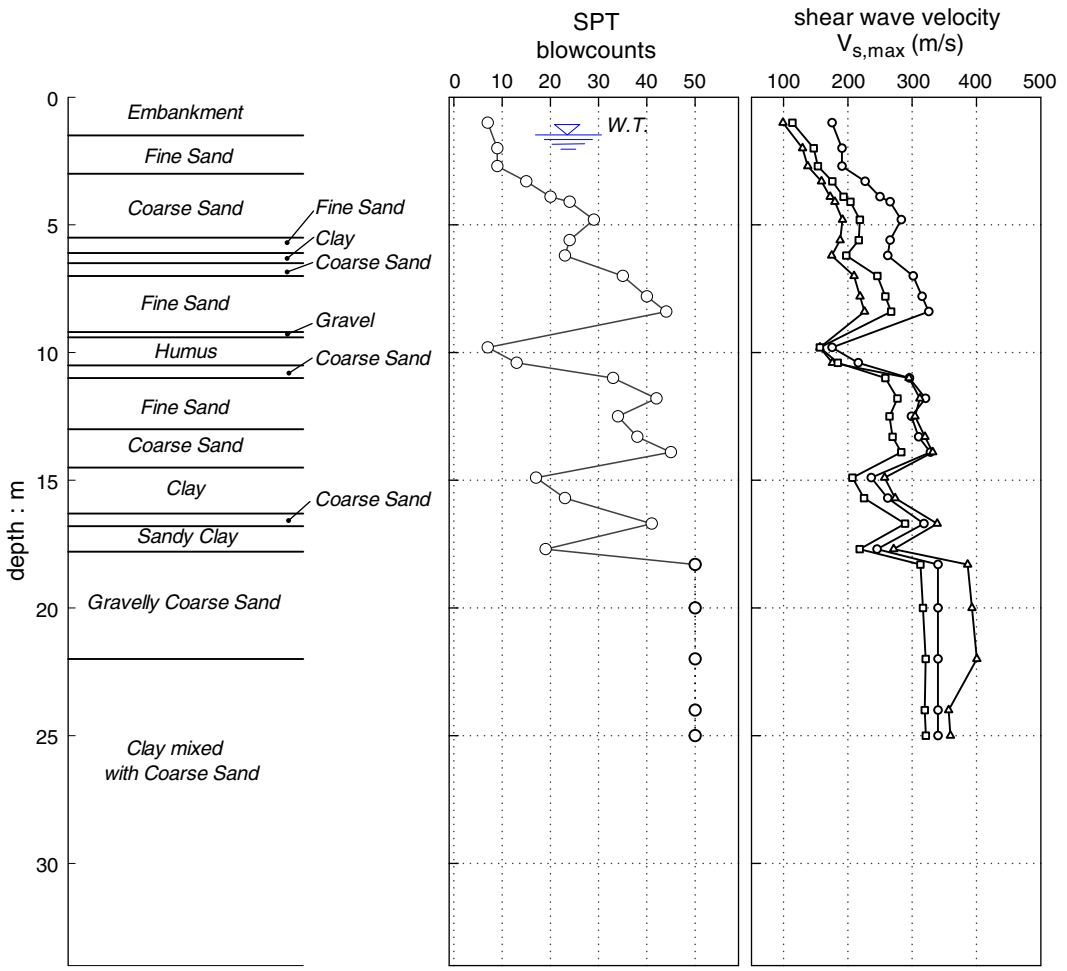

Figure 8. Soil profile, SPT blowcounts and associated shear-wave velocities based on alternative correlations close to pier 138 (SPT data after Iwasaki *et al.* [7]). —○— JSSMFE [49], —△— Seed *et al.* [50], —□— Yoshida *et al.* [38].

stiffer soil to be representative of the ground motion at the Fukae site. The Higashi time history was recorded 35 m below the surface on a stiff soil layer. The synthetic accelerogram was derived by Matsushima and Kawase [34] for the location of the site using a multiple asperity model and considering a 3D basin structure.[‡] Finally, the Motoyama record [35], was recorded at the soil surface, thus it was necessary to be de-convoluted using one-dimensional wave propagation theory [36] to a depth of 20 m, to obtain the pertinent rock motion (hereafter referred to as Motoyama 'rock' motion).

The Motoyama 'rock' motion, along with the Higashi and the Synthetic are plotted in Figure 10 next to the corresponding acceleration spectra. Note the good agreement in the

[‡]The time history was obtained at the Fukae area, on the surface of a 'reference' rock stratum with $V_{s,max} = 400$ m/s.

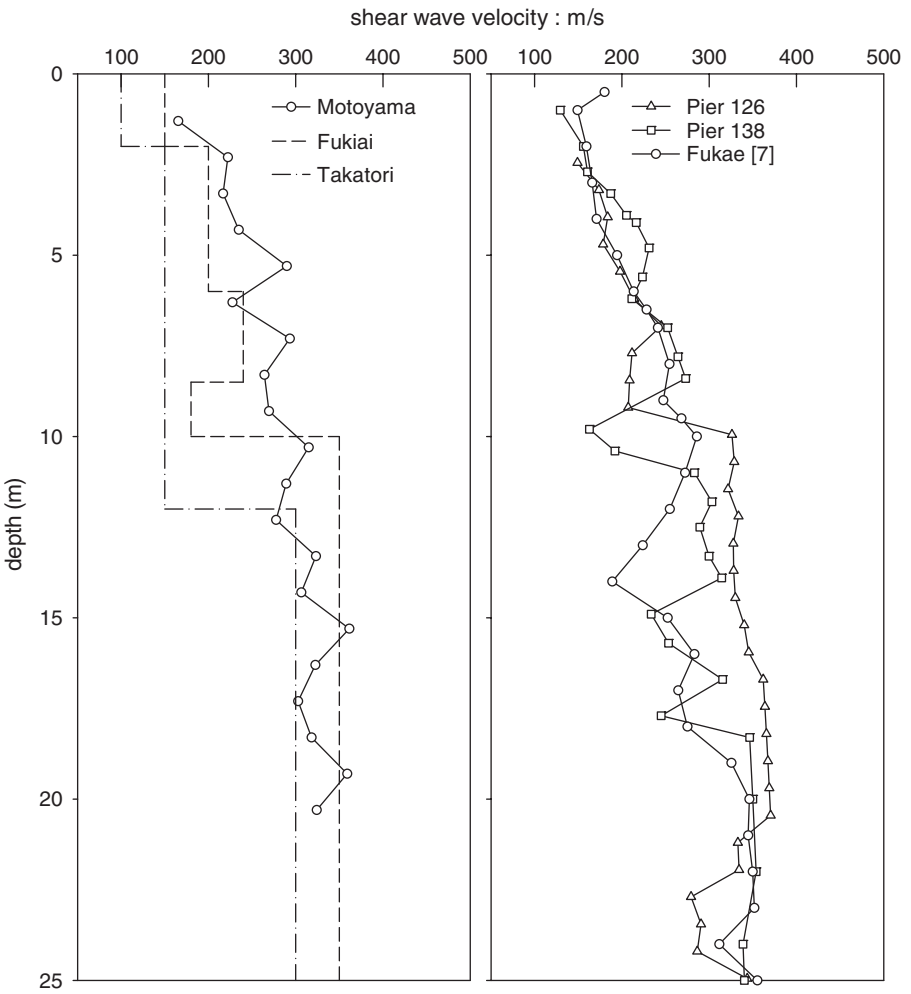

Figure 9. Low-strain shear wave velocities at different sites in Kobe.

Table I. Soil conditions at recording stations and peak characteristics of recorded motions.

Station name	Average V_s (m/s)	Average N	Site class [33]	PGA (g)	PGV (cm/s)
Takatori	180	—	D-E	0.68	169
Fukiai	274	—	D	0.83	115
JMA	385	—	C	0.83	96
Motoyama	277	40	D	0.62	75
Higashi	—	—	'C'	0.44	81
Bridge site (Pier 138)	250	23	D	—	—

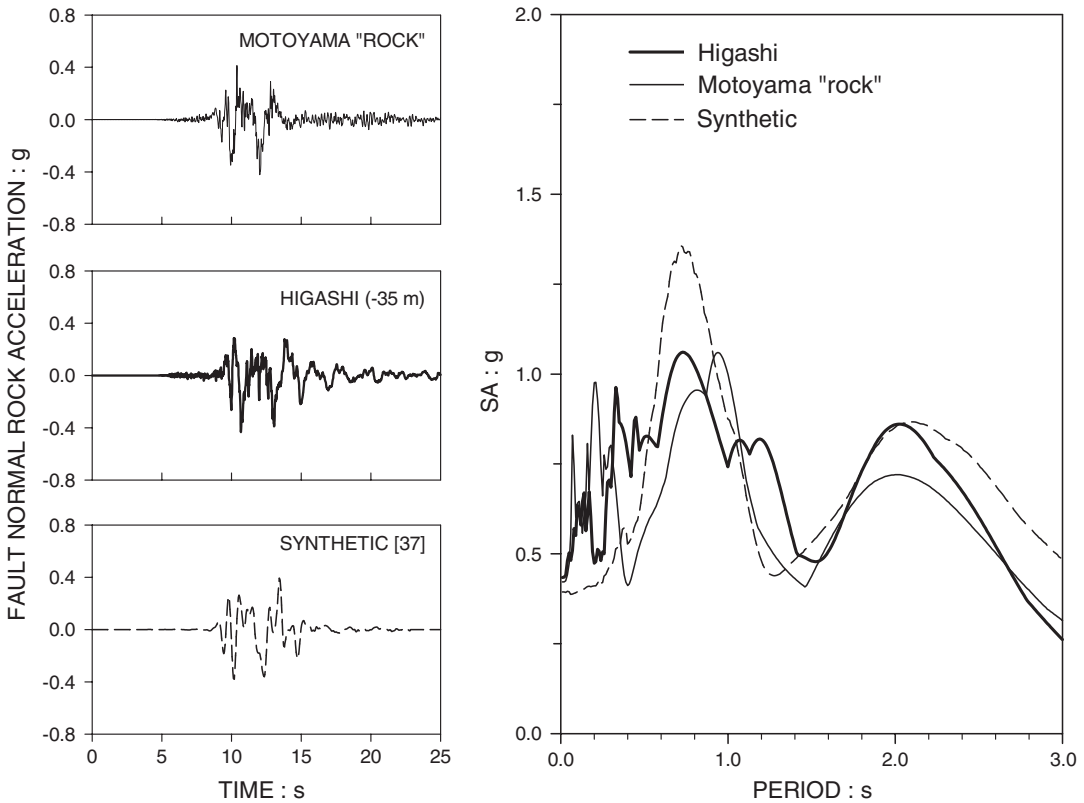

Figure 10. Fault-normal bedrock motions close to the bridge site, and corresponding 5%-damped acceleration spectra.

waveforms and spectra of the three rock motions. Based on this agreement between the three rock motions, and the inherent approximations in the analysis, a more sophisticated de-convolution analysis [37] was not deemed necessary for the Motoyama record.

As a next step, the rock motions were convoluted using one-dimensional wave propagation theory [36] to derive free-field surface motions at the bridge site (Figure 8). To account for the uncertainty in rock elevation, three rock depths (25, 50, 75 m) were considered. The first depth is consistent with the thickness of holocene deposits in the area [25]. The last is a probable upper bound of total thickness of alluvium and diluvium material. The depth of 50 m was selected as a best-estimate scenario. The resulting surface motions are shown and discussed later in this paper. Shear wave velocities were derived from SPT data based on different correlations (Figure 8). The correlation by Yoshida *et al.* [38] was adopted in the analyses.

In Figure 11, corresponding amplification spectra (RRS) in the fault-normal direction between surface and rock are shown for the three amplified records. For each record, three different curves are presented, corresponding to different site thicknesses. As expected, the deeper profiles exhibit peak amplifications at longer periods. It is evident that the actual

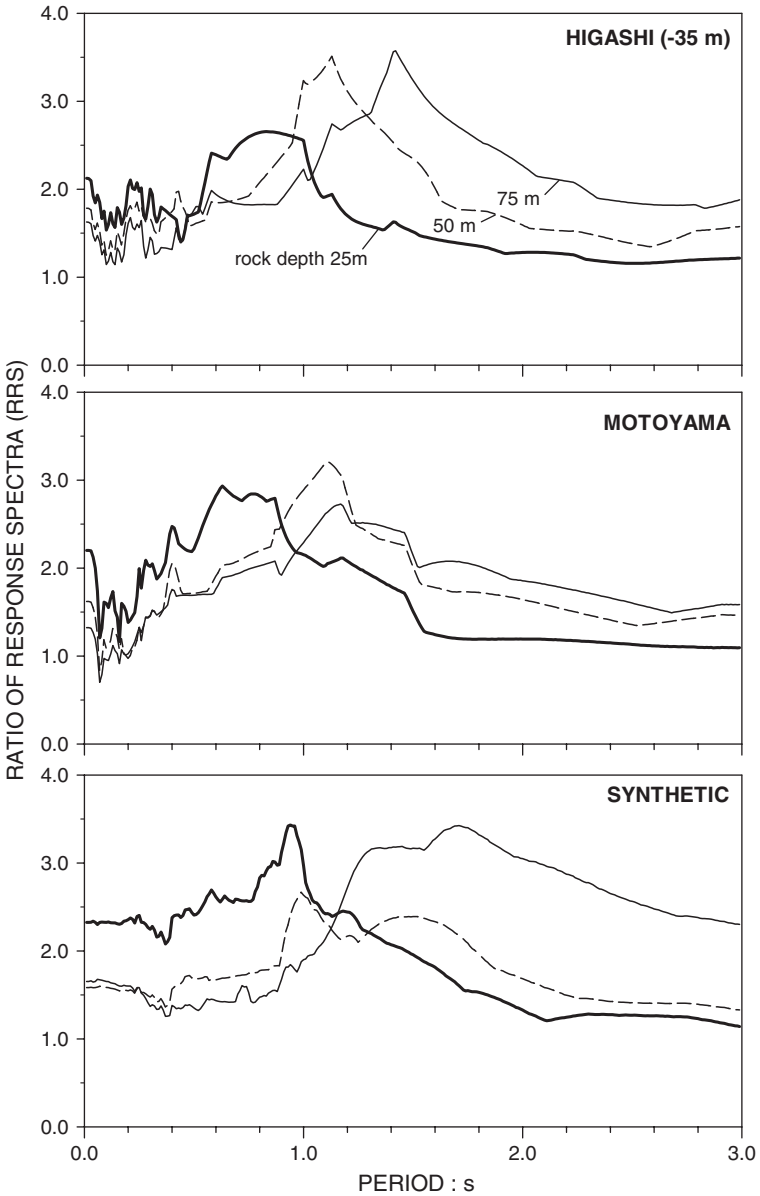

Figure 11. Ratio of response spectra between surface and rock motions along fault-normal direction; $\zeta = 5\%$.

motions (Higashi and Motoyama) exhibit similar amplification patterns. The amplified motions (hereafter referred to as Higashi amplified and Motoyama amplified motion) derived from these records for an average site thickness of 50 m are used in the rest of the paper. It is noted that these motions may loose accuracy at long periods (beyond about 1.5 s), as 2D

effects have not been taken into account. However, this deficiency is deemed of secondary importance for the dynamic analysis of the bridge.

RESPONSE OF FOUNDATION-SUPERSTRUCTURE SYSTEM

The collapsed segment consisted of 18 single, circular piers (P126 to P143), measuring about 12 m in height and 3.1 m in diameter,[§] founded on groups of 17 cast-in-place concrete piles (Figures 1 and 2). The piers were monolithically connected to a two-hinge prestressed concrete deck spanning a length of 35 m. The pile heads were connected to a large cap of dimensions 9.6 m × 10.6 m × 2.1 m. Post-failure laboratory investigations provided an average concrete strength of 35 kPa and a Young's modulus of 28 GPa. For steel reinforcement, the corresponding figures were 5.3 MPa (yield at 3.5 MPa) and 200 GPa, respectively [10].

Longitudinal reinforcement in the pier consisted of three concentric rings composed of 60 D35 mm (#11) bars, a total of 180 bars at the bottom of the columns. The inner ring was terminated at 2.5 m above the pile cap, leaving 120 bars which continued to the top of the pier. Transverse reinforcement consisted of three hoops of D 16 mm (#5). The inner hoop was spaced at 400 mm and stopped 2.5 m above the cap. The two outside hoops were spaced at 200 mm for the first 2.5 m, then spaced at 300 mm.

Structural parameters for the foundation-superstructure system used in previous studies are summarized in Table II. Despite the differences in cross-sectional moment of inertia and (especially) stiffness of the bridge piers among the various studies, the variation in fixed-base natural period (T_{fixed}) is rather small, ranging between 0.55 and 0.75 s. Studies considering SSI provided longer natural periods (T_{SSI}) varying between 0.75 and 0.93 s. Differences in pier strength are considerable, with the normalized yielding strength C_y ($=F_y/M/g$) ranging between 0.5 and 0.7, depending primarily on the assumed concrete strength and structural mass (M). This strength is deemed high given the year of the design (1964) and the adopted seismic coefficient of 0.2 [10]. Estimated displacement ductility capacity (μ_{capacity}) of the pier ranges between 1.6 and 3.2, depending on the assumptions.

Following earlier studies, a single pier model was adopted, as shown in Figure 12. This idealization is justified because of: (i) the almost identical geometry the piers in the segment; (ii) the presence of moment releases in each span; (iii) the uniform ground conditions along the bridge; (iv) the almost identical failure pattern observed in all piers. Two different boundary conditions were examined, fixed and flexible base, as indicated in Figure 12. The first model (also referred to as fixed base model) incorporates two degrees of freedom (deck translation and rotation); the second model (referred to as flexible base or SSI model) incorporates four degrees of freedom (translation and rotation of bridge deck and pier base). In addition, a more detailed DRAIN-2DX model was developed [40], which will be discussed later on. For the purposes of this investigation, the pier is considered elastic or elastic-fully plastic. The structure is excited in the direction perpendicular to the bridge axis (out-of-plane or fault normal direction), which coincides with the direction of maximum ground motion and structural failure. Response to vertical ground motion was found to be small, as it induces dynamic vertical normal stresses in the pier of approximately 2% the design strength of

[§]These dimensions correspond to Pier 138, which is analysed here.

Table II. Structural parameters used in previous studies.

Reference model	Seible *et al.* [8] Single pier on rigid foundation	Park [9] Single pier on rigid foundation	Kawashima and Unjoh [10] Multiple piers on flexible foundation	Michaelides and Gazetas [39] Single pier on flexible foundation	Anastasopoulos [11] Single pier on flexible foundation	Sun *et al.* [14] Single pier on rigid foundation
L (m)	12.3	12	—	11	12	13.5
d (m)	3.1	3.1	3.1–3.3	3.1	3.1	3.3
E (GPa)	—	30.1	27.8	20	25	—
I/I_{gross}	0.4	0.45	0.59	0.75	1	—
K_{pier} (MN/m)	80	107	128	155	157	126
M^{*}_{deck} (Mg)	1100	1121	—	1200	1100	1262
I_{deck} (Mg m^2)	0	0	—	40 000	40 000	—
M_{cap} (Mg)	0	0	—	0	0	—
I_{cap} (Mg m^2)	0	0	—	0	0	—
T_{fixed} (s)	0.75	0.64	0.55[†]	0.68	0.68	0.63
T_{SSI} (s)	—	—	0.75	0.93	0.93	—
F_y (kN)	5407	6640	4673	8240 (bottom)	7280 (bottom)	— —
C_y	0.5	0.6	0.43[†]	0.7	0.66	—
Force–displacement relation	—	Elastic-perfectly plastic	Takeda	Elastic-perfectly plastic	BIAX (Park)	Extended distinct element method
α	—	0	0.07–0.15	0	0	—
ζ_{pier} (%)	—	5	—	5	5	3
ζ_{SSI} (%)	—	—	—	7.5	7.5	—
$\mu_{capacity}$	2.4	2.2	3.2	1.6	3.6	3.9
Excitation	—	JMA	JMA	JMA, Fukiai	JMA, Fukiai, Takatori	JMA
μ_{demand}	—	> 2.2	> 3.2	1.3–1.7	> 3.6	> 3.9

—not reported.

[*] Includes portion of pier mass.

[†] Estimated by the authors considering $M_{deck} = 1100$ Mg.

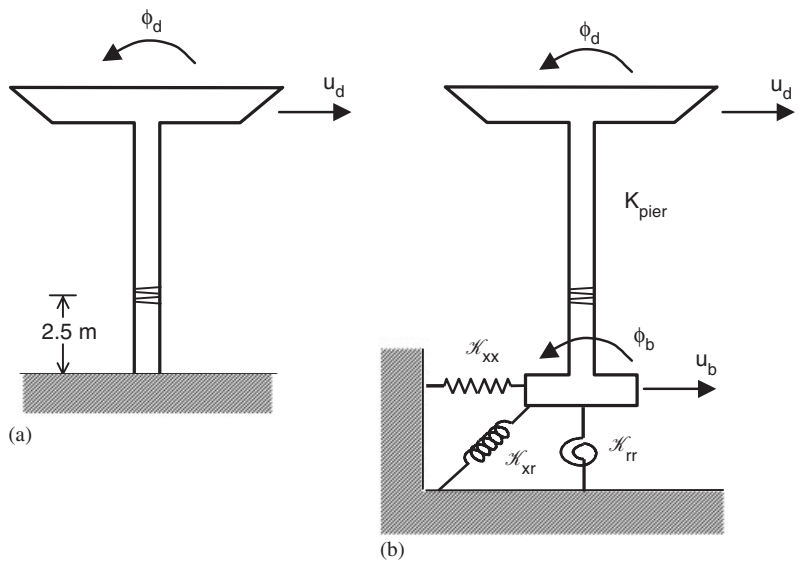

Figure 12. Pier models used in this study: (a) fixed-base pier with two degrees of freedom; and (b) pier on flexible base with four degrees of freedom.

unconfined concrete [41]. Similarly, $P-\Delta$ effects were found to affect the pre-failure response of the massive pier by an insignificant amount (about 1%). In subsequent analyses, both vertical excitation and $P-\Delta$ effects are neglected.

Vibrational characteristics of fixed-base pier

Detailed calculations performed by the authors suggest a participating deck mass (M_{deck}) of about 1000 Mg, a rotational deck moment of inertia (I_{deck}) of approximately 32 300 Mg m^2, and a pier mass (M_{pier}) of about 226 Mg (Table III). Following Seible *et al.* [8], the cross-sectional moment of inertia of the cracked pier was taken at approximately 40% of its gross value. Using this information, the fixed-base natural period of the bridge (modelled as a generalized, single degree of freedom—SDOF—oscillator), can be estimated from the Rayleigh quotient [16, 42, 43]

$$T_{\text{fixed}} = 2\pi\sqrt{\frac{M_{\text{deck}} + \phi_M M_{\text{pier}} + \phi_D^2 I_{\text{deck}}}{K_{\text{pier}}}} \tag{1}$$

in which $K_{\text{pier}} = 3EI/L^3$ denotes the flexural stiffness of the cantilever ('flag-pole') pier. The dimensionless coefficients ϕ_M and ϕ_D account for the participation in overall inertia of pier mass (M_{pier}) and rotational inertia of the deck (I_{deck}). They are computed from the following

Table III. Structural and SSI parameters considered.

L (m)			12		
d (m)			3.1		
E (GPa)			27.8		
I/I_{gross}	0.4	0.5	1	0.5	0.5
K_{col} (MN/m)	88	109	219	109	109
M_{deck} (Mg)	1000	1000	1000	1000	1000
I_{deck} (Mg m^2)	32 300	32 300	32 300	0	0
M_{cap} (Mg)	750	750	750	750	0
I_{cap} (Mg m^2)	9000	9000	9000	0	0
M_{pier} (Mg)	226*	226*	226*	226*	226*
K_{xx} (MN/m)			310 (950)†		
K_{xr} (MN)			1090 (3750)†		
K_{rr} (MN m)			48 300 (70 000)†		
ζ_{xx}			0.31 (0.11)†		
ζ_{xr}			0.20 (0.08)†		
ζ_{rr}			0.03 (0.03)†		
T_{fixed} (s)	0.84	0.75	0.53	0.62	0.62
T_{SSI} (s)	1.04	0.98	0.84	0.89	0.87
ζ_{SSI} (%)	9.8	10.5	12.4	10.5	10.5
χ_{fixed}	0.70	0.70	0.70	1.03	1.03
χ_{SSI}	0.94	0.97	1.04	1.16	1.04

*Participating mass: $(\frac{33}{140}) \times 226$ Mg $= 53$ Mg.

†Estimated by Michaelides and Gazetas [39].

energy expressions:

$$\phi_M = \frac{1}{L}\int_0^L \psi^2 \, \mathrm{d}x \tag{2}$$

$$\phi_D = \left.\frac{\mathrm{d}\psi}{\mathrm{d}x}\right|_{x=L} \tag{3}$$

where $\psi = \psi(x)$ stands for the deflected shape of the pier as a function of height, varying from 0 at the base to 1 at the point of maximum deflection.

For fixed-base conditions, it is sufficient to assume

$$\psi(x) = \frac{1}{2}\left(\frac{x}{L}\right)^2 \left[3 - \left(\frac{x}{L}\right)\right] \tag{4}$$

which corresponds to the deflected shape of a uniform elastic column subjected to a static lateral head force. In the above equation, x denotes the elevation measured from the base of the column.

Equations (1)–(4) yield the period of a fixed base pier (T_{fixed}), taking into account the rotational inertia of the deck (I_{deck}) and a distributed (instead of lumped) pier mass (M_{pier}).

$$T_{fixed} = 2\pi\sqrt{\frac{M_{deck} + \left(\frac{33}{140}\right) M_{pier} + (3/2L)^2 I_{deck}}{K_{pier}}} \tag{5}$$

For a typical Hanshin pier at Fukae section, Equation (5) yields,

$$T_{\text{fixed}} \cong 0.84 \text{ s} \tag{6}$$

as shown in Table III. The increase in period relative to the periods listed in Table II is attributed to the inclusion of the rotational inertia of the deck. Note in this regard, that the overall effective mass of the bridge deck (M) according to the present analysis is

$$M = 1000 \text{ Mg} + \left(\frac{33}{140}\right) \times 226 \text{ Mg} + \left(\frac{3}{2 \times 12 \text{ m}}\right)^2 \times 32300 \text{ Mg m}^2 = 1557 \text{ Mg} \tag{7}$$

nearly 40% higher than in the aforementioned studies.

Owing to the presence of deck rotational inertia and pier mass, the following participation factor (χ) for the generalized mode needs to be considered:

$$\chi = \frac{M_{\text{deck}} + ((1/L)\int_0^L \psi(x)^2 \, \mathrm{d}x) M_{\text{pier}}}{M} \tag{8}$$

pertaining to horizontal ground excitation [44]. The above factor implies that only a portion of the mass of the system (M) is mobilized under horizontal ground shaking. (This in contrast to the SDOF oscillator which does not incorporate rotational inertia and, thereby, its participation factor always equals 1.)

Equation (8) yields

$$\chi \cong 0.70 \tag{9}$$

which elucidates the role of deck rotational inertia in reducing the effective earthquake input in the system. A rigorous eigenvalue analysis performed by the authors suggests that the error in the above estimate as compared to the 'exact' period of multi-degree of freedom pier is only about 2% in the first mode. The same analysis showed that the second mode of the system has a negligible contribution to the response.

Vibrational characteristics of pier on flexible base

The compliance of foundation further increases the natural period (T_{SSI}) and damping (ζ_{SSI}) of the system. Modelling the bridge as a generalized SDOF oscillator accounting for the horizontal translation and rotation both of the superstructure and the pile cap, good estimates of natural period (T_{SSI}) and damping (ζ_{SSI}) can be obtained from the energy expressions [16, 43]:

$$T_{\text{SSI}} = 2\pi \sqrt{\frac{M_{\text{deck}} + \phi_M M_{\text{pier}} + \phi_{21}^2 M_{\text{cap}} + \phi_{31}^2 I_{\text{deck}} + \phi_{41}^2 I_{\text{cap}}}{\phi_K K_{\text{pier}} + \phi_{21}^2 K_{xx} + \phi_{41}^2 K_{rr} + 2\phi_{21}\phi_{41} K_{xr}}} \tag{10}$$

$$\zeta_{\text{SSI}} = \frac{\phi_K K_{\text{pier}} \zeta_{\text{pier}} + \phi_{21}^2 K_{xx} \zeta_{xx} + \phi_{41}^2 K_{rr} \zeta_{rr} + 2\phi_{21}\phi_{41} K_{xr} \zeta_{xr}}{\phi_K K_{\text{pier}} + \phi_{21}^2 K_{xx} + \phi_{41}^2 K_{rr} + 2\phi_{21}\phi_{41} K_{xr}} \tag{11}$$

In the above equations, K_{pier}, M_{pier}, and ζ_{pier} correspond to the stiffness, mass and damping of the pier, K_{xx}, K_{xr}, K_{rr}, ζ_{xx}, ζ_{xr} and ζ_{rr} correspond to the horizontal, cross-term and rotational stiffness and damping of the foundation, and M_{deck}, M_{cap}, I_{deck} and I_{cap} correspond to the deck and pile cap mass and rotational mass of inertia accordingly.

The coefficients ϕ_{21}, ϕ_{31}, ϕ_{41}, and ϕ_M are dimensionless weight factors given by

$$\phi_{21} = K_{\text{pier}}(K_{rr} + K_{xr}L)\lambda^{-1} \tag{12a}$$

$$\phi_{31} = \left[(1 - \phi_{21})\frac{3}{2L} + \frac{1}{2}\phi_{41}\right] \tag{12b}$$

$$\phi_{41} = K_{\text{pier}}(K_{xr} + K_{xx}L)\lambda^{-1} \tag{12c}$$

$$\lambda = (-K_{xr}^2 + K_{rr}K_{xx}) + K_{\text{pier}}[K_{rr} + (2K_{xr}L + K_{xx}L^2)] \tag{12d}$$

$$\phi_M = \frac{1}{L}\int_0^L (\psi_{\text{SSI}}(x))^2 \, \mathrm{d}x \tag{12e}$$

$$\phi_K = \frac{L^3}{3}\int_0^L \left(\frac{\mathrm{d}^2\psi_{\text{SSI}}}{\mathrm{d}x^2}\right)^2 \mathrm{d}x \tag{12f}$$

In the above equations, ψ_{SSI} is a modified shape function expressing the deflected shape of the flexibly supported structure under a static lateral seismic load. It relates to the fixed-base shape function $\psi(x)$ of Equation (4) through the expression

$$\psi_{\text{SSI}}(x) = (1 - \phi_{21} + L\phi_{41})\psi(x) + \phi_{21} - x\phi_{41} \tag{12g}$$

The above formulation is discussed in a companion paper [43] and in the Dissertation of Syngros [16].

Equations (10) and (11) differ from similar formulations developed for structures on surface foundations [45, 46] due to the presence of cross terms K_{xr} and ζ_{xr} in the foundation impedance, and rotational inertia in the deck (I_{deck}) and pile cap (I_{cap}). These parameters are important for the specific structure, given the large rotational inertia of the mushroom-like ('Pilz') deck, the massive pile cap and the presence of piles in the foundation. Note that for the limiting case of infinite foundation stiffness (fixed base), Equation (10) duly reduces to Equation (1). Similarly to the fixed base oscillator, the participation factor of the generalized flexible base oscillator is given by

$$\chi_{\text{SSI}} = \frac{M_{\text{deck}} + ((1/L)\int_0^L \psi_{\text{SSI}} \, \mathrm{d}x)M_{\text{pier}} + \phi_{21}M_{\text{cap}}}{M} \tag{13}$$

where M denotes the total effective mass (numerator in right-hand side of Equation (10)).

Using the finite-element code K-PAX [16] in conjunction with the pile-to-pile interaction model of Mylonakis *et al.* [47], estimates of foundation stiffness have been obtained as shown in Figure 13 and Table III. The selected values correspond to low-excitation frequencies (less than 2 Hz) and peak shear strains in the free-field of approximately 5×10^{-3}, which are consistent with the levels of strain imposed by the input motions. Corresponding values for low strains obtained by Michaelides and Gazetas [39] are provided in parenthesis. The differences between the predictions, particularly in the swaying mode, are as expected.

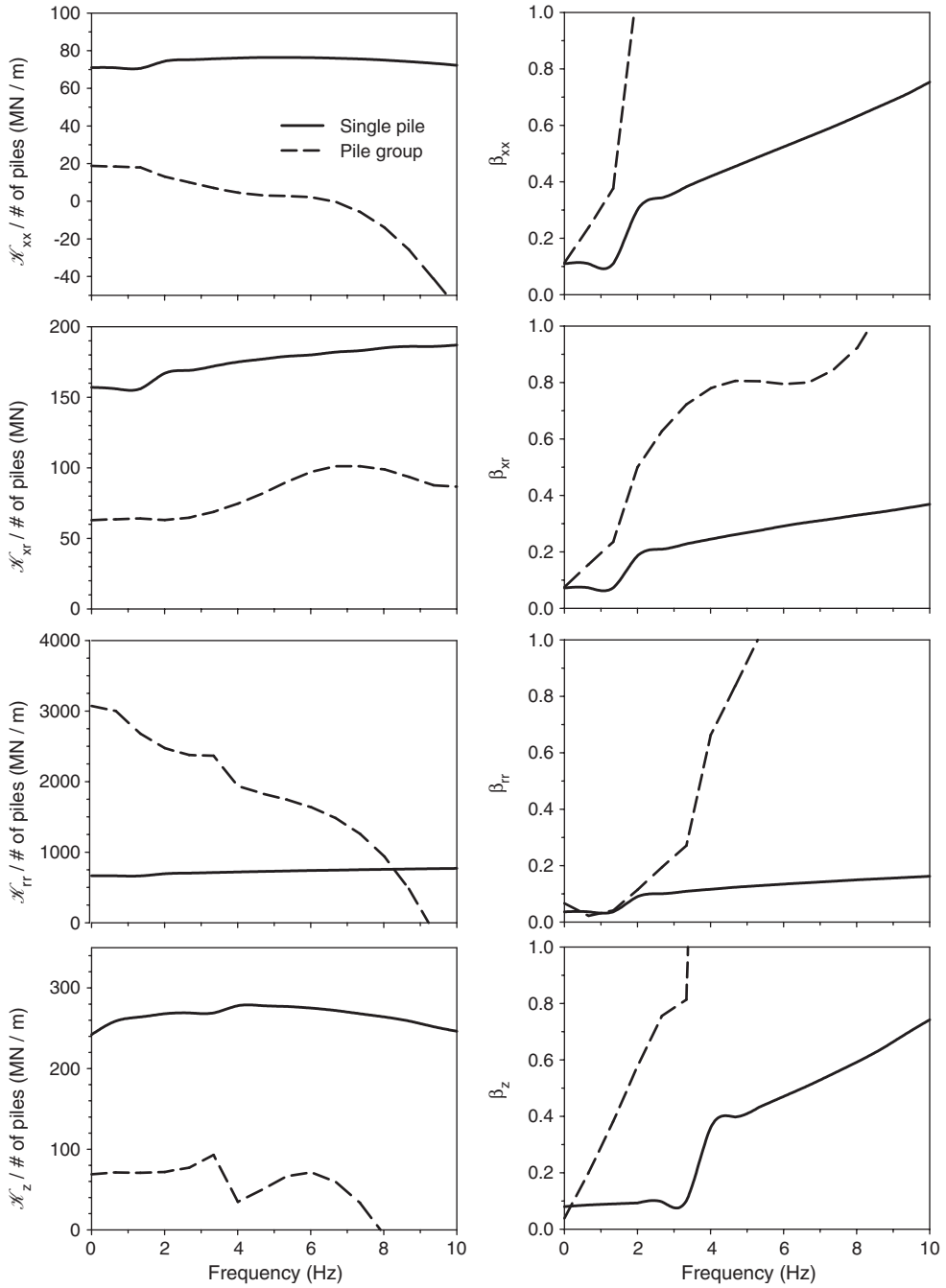

Figure 13. Stiffness and damping ratio for a single pile and the 17-pile group of pier 138.

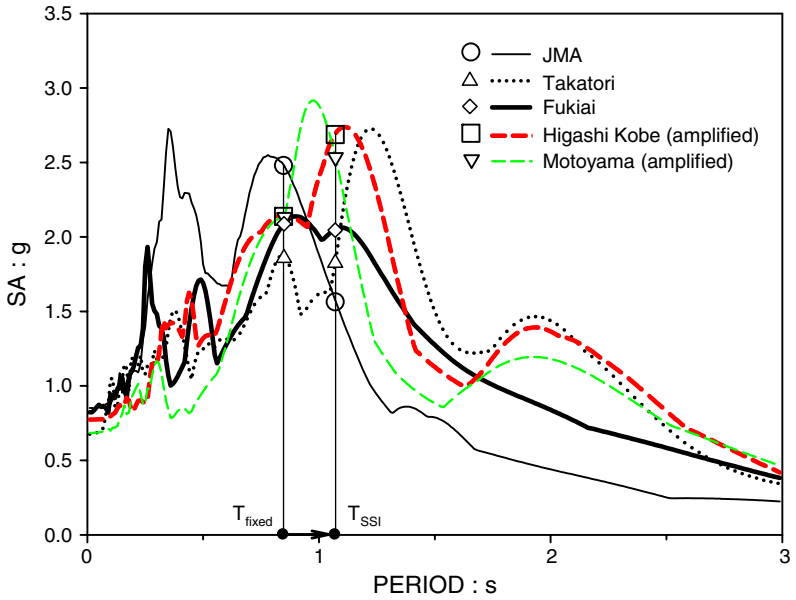

Figure 14. Acceleration response spectra of selected ground motions in the fault normal direction; $\zeta = 5\%$.

Based on the parameters in Table III, the natural period, damping, and modal participation factor of the flexibly-supported system are estimated from Equations (10) to (13) as

$$T_{SSI} = 1.04 \text{ s} \tag{14}$$

$$\zeta_{SSI} = 0.098 \text{ or } 9.8\% \tag{15}$$

$$\chi_{SSI} = 0.94 \tag{16}$$

which are indicative of the role of SSI in increasing natural period by 20%, damping ratio by 100% and modal participation factor by 30% compared to the fixed base oscillator. Note that the damping estimate in Equation (15) is a *lower bound*, as it does not account for inelastic action in the pier.

Simplified spectral analysis

From the elastic spectra of Figure 14, the influence of SSI on the response starts becoming apparent. For instance, if the actual excitation at the Fukae site was similar to the JMA record, the increase in period due to SSI and the progressive cracking of the pier would tend to slightly reduce the response, as indicated by the decreasing trend of the spectrum beyond about 0.8 s. In contrast, with either Fukiai or Takatori motions (undoubtedly more likely surrogate motions to the unknown real ones at the Fukae site), SSI would lead to equal or higher response. The trend becomes more apparent with the Higashi and Motoyama amplified records (site thickness of 50 m), for which elastic response at T_{SSI} may exceed 2.5 g.

As a first approximation, for the somewhat conservative estimate of $SA \approx 0.94 \times (2.1g) \times (5/9.8)^{0.4} = 1.51g$, which is derived from Fukiai spectrum and accounts for both the participation factor of the generalized mode and the increased damping due to SSI (Table III), the force reduction factor (R) based on a calculated strength ratio C_y of the column of about 0.5 g would be equal to approximately $1.51g/0.5g \approx 3$. Taking the *equal displacement* rule as approximately valid [9, 15, 44], the ductility demand on the system, $\mu^{(\text{system})}{}_{\text{demand}}$, would be

$$\mu^{(\text{system})}{}_{\text{demand}} \approx R \approx 3 \tag{17}$$

The ductility demand on the *pier*, $\mu^{(\text{pier})}{}_{\text{demand}}$, is obtained by considering only pier deformations.¶ For an elastic-perfectly plastic system, this can be achieved by means of the expression [15]

$$\mu^{(\text{pier})} = (1 + c)\mu^{(\text{system})} - c \tag{18}$$

where c is a dimensionless factor expressing the relative flexibility of foundation and superstructure

$$c = K_{\text{pier}} \frac{L^2 K_{xx} + 2LK_{xr} + K_{rr}}{K_{xx}K_{rr} - K_{xr}^2} \tag{19}$$

For the problem at hand, $c = 0.76$; thus,

$$\mu^{(\text{pier})}{}_{\text{demand}} = (1 + 0.76) \times 3.1 - 0.76 = 4.7 \tag{20}$$

which is 50% higher than system ductility and far exceeds the ductility capacity (μ_{capacity}) of the pier (Table II).

On the other hand, ignoring SSI and for the conservative elastic estimate of

$$SA \approx 0.70 \times 2.1g = 1.47g \tag{21}$$

which accounts for the modal participation factor of the generalized system in Table III, the spectra of Figure 14 would yield a ductility demand of

$$\mu^{(\text{pier})}{}_{\text{demand}} \approx R = \frac{1.47g}{0.5g} \approx 3 \tag{22}$$

which, although conservatively estimated, lies within the probable range of ductility capacity (2.2–3.2) in Table II and, therefore, could hardly explain the spectacular failure of the bridge.

Although approximate, the above results indicate a detrimental role of soil in the piers' collapse. The ductility demand of the piers accounting for SSI appears to be higher when compared to the demand imposed to a fixed base pier. These results, based on simple 'elastic' methods are verified with the following more advanced analyses.

¶Recall that the response of a flexibly-supported pier involves rigid body movements, which do *not* inflict structural damage. Design implications of this effect are discussed in References [15, 48].

Nonlinear dynamic analyses

To gain further insight on the role of SSI in the inelastic response of the pier, a series of non-linear time-domain inelastic analyses were conducted. As a first step, a fixed-base SDOF oscillator was considered. Results for three excitation motions and three pier strengths are provided in Figure 15, plotted in terms of ductility demand versus elastic structural period.

To account in an approximate manner for the effect of rotational inertia of the deck (which is not incorporated in the SDOF system), the input acceleration is multiplied by the participation factor of the generalized simple oscillator (i.e. $\chi \cong 0.70$—see Equation (9)). Another approach is to consider the modified oscillator strength, of

$$C_y^* = C_y/\chi = 0.5/0.70 = 0.71 \tag{23}$$

which is about 40% higher than the actual yielding strength. This increase in strength suggests a beneficial influence of the rotational inertia of the deck for structures of this type.

For flexible base conditions, the corresponding strength is (Equation (16)):

$$C_y^* = C_y/\chi_{\mathrm{SSI}} = 0.5/0.94 = 0.53 \tag{24}$$

As a result, the ductility demand in the fixed-base pier for JMA, Fukiai, and Takatori records is about 2, 3 and 2.2, respectively. For the flexible-base system, considering, as an approximation, an 'equivalent' SDOF system with a modified natural period and strength, the corresponding system ductilities are read from Figure 15 at approximately 2.2, 3.3 and 4.

The ductility demand in the pier can be extracted from the above values by means of Equation (18). This yields the estimates of 2.9, 5 and 6.3 for the three records, respectively.

Although approximate, the above analysis indicates a strong detrimental influence of SSI in inelastic response. This is in agreement with the previous discussions (except for the observed increase for the JMA motion). The results for Fukiai motion ($\mu_{\mathrm{fixed}} = 3, \mu_{\mathrm{SSI}} = 5$) are in accord with those in Equations (22) and (30).

Proceeding to a more advanced model, a MDOF inelastic model of the pier was developed using the computer code DRAIN-2DX [40, 42]. In this model, the column was divided into four two-noded inelastic beam elements, each having one translational and one rotational degree of freedom at each end. Concentrated plasticity at the ends of the elements was adopted. The influence of shear forces in the development of plastic deformation was neglected. The compliance of the foundation was modelled using a series of springs and dashpots attached to the base of the pier (Figure 12). Assuming initial yielding 2.5 m above the top of the pile cap, a yielding force of 5636 kN was established corresponding to a deck acceleration of about 0.5 g. The inherent (non-SSI) damping of the structure was assumed of the Rayleigh type, taken equal to 5% of critical. Eigenvalue analyses provided the values $T_{\mathrm{fixed}} = 0.88$ s and $T_{\mathrm{SSI}} = 1.07$ s which are in good agreement with the results of the simplified model in Table III. The SSI dashpots on each degree of freedom were computed from the linear coefficients ζ_{ij} of the foundation impedance, at the characteristic period T_{SSI} (Figure 13). Results obtained with five earthquake records are depicted in Table IV.

Using the JMA record as the foundation input motion (FIM), SSI appears to play a beneficial role, as column ductility demand decreases from 2.5 for the fixed-base pier to 2.2 for the flexibly supported one (Table IV). In contrast, using the Fukiai and Takatori motions as FIM's, SSI is clearly detrimental, increasing substantially the ductility demand in the pier. In the case of the Fukiai record, the agreement between the numerical results of ductility

Table IV. Tabulated results from DRAIN-2DX and simplified analyses of inelastic bridge response.

Excitation	Pier ductility demand		Increase (%)		Role of SSI	Predicted performance
	Fixed base (A)	Deformable base (B)	DRAIN-2DX (columns A,B)	Simple model (Equations (17)–(22))		
Fukiai	3.1	4.1	+32	+54	Detrimental	Failure
Takatori	3.2	7.3	+128	+42	Very detrimental	Failure
Motoyama*	3.5 to 3.7	3.2 to 3.5	−5 to −9	+92	≈ Minor	Probably failure
Higashi*	3.9 to 4.6	4.8 to 6.4	+23 to +39	+100	Detrimental	Failure
JMA	2.5	2.2	−12	−12	Slightly beneficial	Heavy damage

*Amplified to account for soil effects.

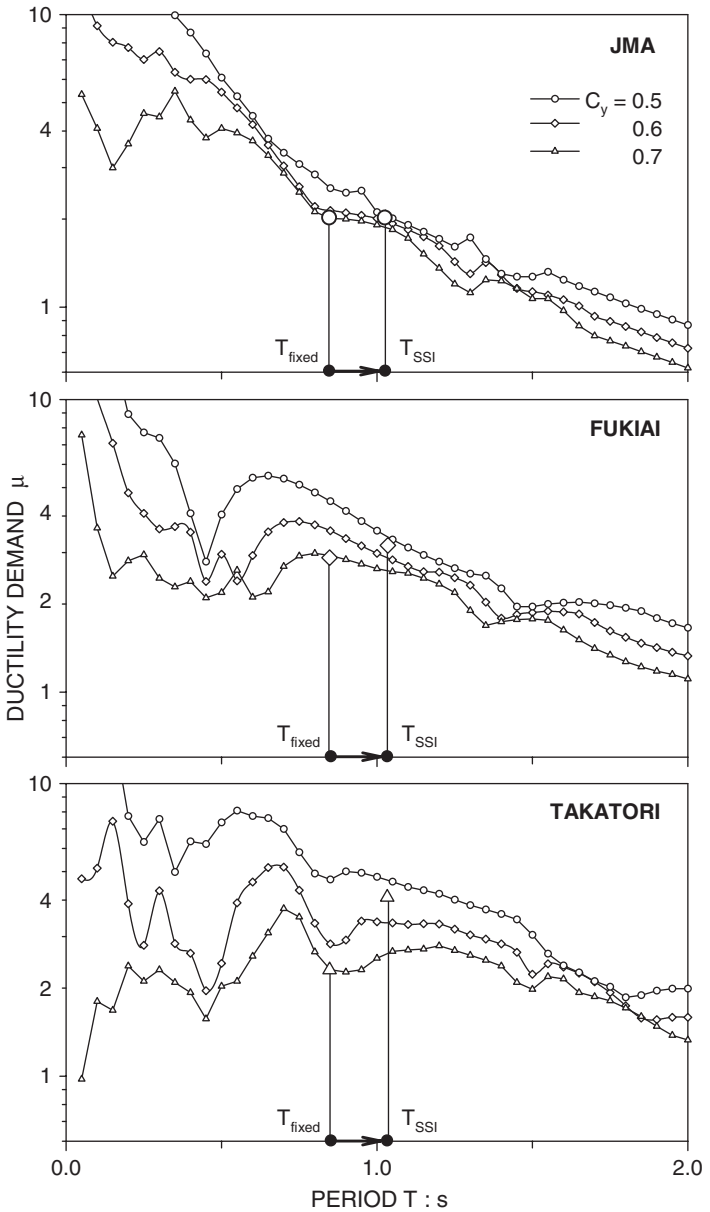

Figure 15. Ductility demand of a SDOF oscillator subjected to the fault-normal component of three main records; $\zeta = 5\%$.

demand (μ) and those in Equations (20) and (22) is encouraging for the simple analysis. The strongest SSI effect is observed with the Takatori record: μ increases from 3.2 for the fixed-base structure to the astonishing 7.3 for the flexibly supported—a detrimental consequence of the strong spectral peak at about $T \approx 1.2$ s (Figure 14).

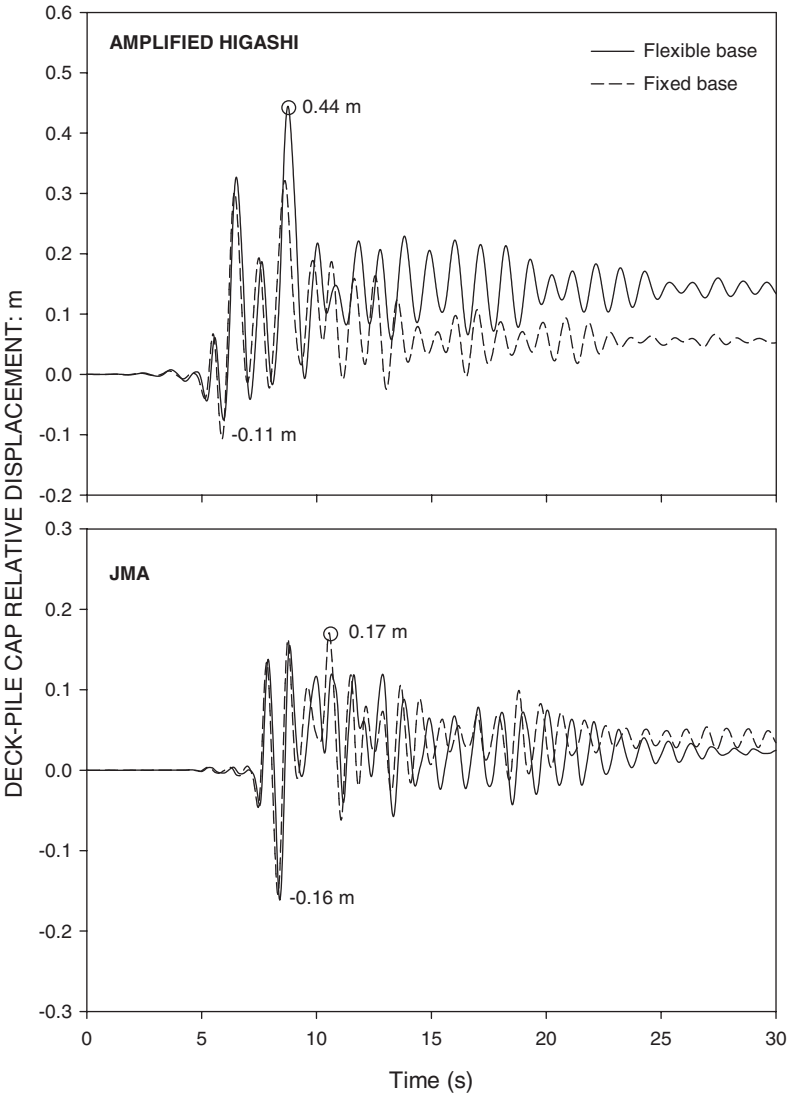

Figure 16. Pile-cap to deck relative displacement from DRAIN-2DX non-linear analyses of flexible and fixed base systems using fault-normal components of JMA and amplified Higashi records.

Substantial increase in ductility demand with SSI is also observed with the amplified Higashi motion (Figure 16), while with the amplified Motoyama motion its role is rather minor. The ranges in computed ductility values for the amplified Motoyama and Higashi motion stem from the different scenarios of soil thickness used in the amplification analyses. Again, the trends obtained with the simple analysis are in qualitative agreement with the numerical study.

The excessive seismic demand computed with the Fukiai, Takatori, and Higashi records may explain the spectacular failure of the 18 piers of the bridge. This suggests that the

actual excitation at the site may have indeed resembled the Fukiai, Takatori, or amplified Higashi–Kobe motions much more than the JMA or amplified Motoyama accelerograms.

CONCLUSIONS

Analytical and recorded evidence is presented on a quadruple detrimental role of soil in the collapse of Hanshin Expressway at Fukae. *First*, the soil modified the incoming seismic waves such that the resulting ground surface motion became very severe for the particular bridge. *Second*, the presence of compliant soil at the foundation resulted to an increase in natural period of the bridge, which moved *it* to a region of stronger response; *Third*, the compliance of the foundation increased the participation of the fundamental mode, also leading to stronger response. *Fourth*, ductility demand in the pier was higher than the ductility demand of the system, as suggested by Equation (20). All four phenomena might have simply worsen an already dramatic situation for the bridge due to its proximity to the fault and the structural deficiencies of the pier which were almost unavoidable given the time of design of the bridge (1964). The above findings contradict a widespread view of an always-beneficial role of SSI in seismic response.

ACKNOWLEDGEMENTS

Financial support to the first two authors was provided by the National Science Foundation under U.S.–Japan Collaborative Program (NSF #0000101). The first author also received partial financial support from University of Patras, through a Caratheodory Grant (#B.388). Data were provided by Drs Walter Silva, Yoshinori Iwasaki, Yukio Adachi, Shunichi Kataoka, Shinichi Matsushina, Manabu Nakayama, and others. Their help is gratefully acknowledged. Drs Odysseus Michaelides and Sissy Nikolaou provided valuable help in the early phases of the study. The authors also benefited from the work of Dr Yannis Anastasopoulos, who conducted research on structural aspects of the problem, including retrofit and seismic isolation. Thanks are also due to the anonymous reviewers for many excellent suggestions.

REFERENCES

1. Yamaguchi N, Yamazaki F. Estimation of strong motion distribution in the 1995 Kobe earthquake based on building damage data. *Earthquake Engineering and Structural Dynamics* 2001; **30**(6):787–801.
2. EERI. *Northridge Earthquake Reconnaissance Report*, vol. 1, Earthquake Spectra Supplement to vol. 11, 1995.
3. Werner SD, Dickenson SE. Hyogo-Ken Nanbu earthquake of January 17, 1995: a post-earthquake reconnaissance of port facilities. Committee on Ports and Harbor Lifelines, ASCE: New York, 1995.
4. NIST. The January 17, 1995 Hyogoken-Nanbu (Kobe) earthquake. Performance of structures, lifelines, and fire protection systems. *NIST Special Publication 901*, *ICSSC TR18*, National Institute of Standards and Technology, Gaithersburg, MD, U.S.A., 1996.
5. Japanese Geotechnical Society. Geotechnical aspects of the January 17 1995 Hyogo Ken Nambu earthquake. *Soils and Foundations* (Special issue, December) 1996.
6. Japanese Geotechnical Society. Geotechnical aspects of the January 17 1995 Hyogo Ken Nambu earthquake. *Soils and Foundations* (Special issue, No. 2, September) 1998.
7. Iwasaki T, Fujino Y, Iemura H, Ikeda S, Kameda H, Katayama T, Kawashima K, Onishi Y, Saeki S, Toki K. Report on Highway bridge damage caused by the Hyogo-ken Nanbu earthquake of 1995. Committee on Highway Bridge Damage caused by the Hyogo-Ken Nambu Earthquake, Japan, 1995.
8. Seible F, Priestley MJN, Macrae GA. The Kobe earthquake of January 17, 1995: initial impressions from a quick reconnaissance. *SSRP-95/03*, Structural Systems Research, University of California, San Diego, La Jolla, CA, U.S.A., 1995.

9. Park R. An analysis of the failure of the columns of a 600 meter length of the Hanshin elevated expressway during the great Hanshin earthquake of 17 January 1995. *Bulletin of the New Zealand National Society for Earthquake Engineering* 1996; **29**(2):73–82.
10. Kawashima K, Unjoh S. The damage of highway bridges in the 1995 Hyogo-Ken Nambu earthquake and its impact on Japanese seismic design. *Journal of Earthquake Engineering* 1997; **1**(3):505–541.
11. Anastasopoulos I. Analysis of the failure of two bridges in the 1995 Kobe earthquake, and the role of soil. *Diploma Thesis*, National Technical University, Athens, Greece 1999 (in Greek).
12. Sun L, Goto Y, Hayashi H, Kosa K. Damage mechanism analysis of RC bridge by nonlinear dynamic simulations. *12th World Conference on Earthquake Engineering*, New Zealand, 2000, Paper 0488.
13. Abe S, Fujino Y, Abe M. An analysis of damage to Hanshin elevated expressway during 1995 Kobe earthquake. *12th World Conference on Earthquake Engineering*, New Zealand, 2000, Paper 0318.
14. Sun L, Zhou C, Qin D, Fan L. Application of extended distinct element method with lattice model to collapse analysis of RC bridges. *Earthquake Engineering and Structural Dynamics* 2003; **32**(8):1217–1236.
15. Mylonakis G, Gazetas G. Seismic soil–structure interaction: beneficial or detrimental? *Journal of Earthquake Engineering* 2000; **4**(3):277–301.
16. Syngros C. Seismic response of piles and pile-supported bridge piers evaluated through case histories. *Ph.D. Dissertation*, The City College and the Graduate Center of the City University of New York, New York, 2004.
17. Gazetas G. Foundation vibrations. In *Foundation Engineering Handbook* (2nd edn), Chapter 15, Fang HY (ed.). Van Nostrand Reinholds: New York, 1991; 553–593.
18. Kim S, Stewart JP. Kinematic soil–structure interaction from strong motion recordings. *Journal of Geotechnical and Geoenvironmental Engineering* (ASCE) 2003; **129**(4):323–335.
19. Veletsos AS, Prasad AM, Wu WH. Transfer functions for rigid rectangular foundations. *Journal of Earthquake Engineering and Structural Dynamics* 1997; **26**(1):5–17.
20. Bielak J. Dynamic response of non-linear building-foundation systems. *Earthquake Engineering and Structural Dynamics* 1978; **6**(1):17–30.
21. Resendiz D, Roesset JM. Soil–structure interaction in Mexico City during the 1985 earthquake. In *The Mexico Earthquakes of 1985*, Cassaro MA, Romero EM (eds). ASCE Special Publication: New York, 1987; 193–203.
22. Qian J, Beskos DE. Dynamic interaction between 3-D rigid surface foundation and comparison with the ATC-3 provisions. *Earthquake Engineering and Structural Dynamics* 1995; **24**:419–437.
23. Takewaki I. Remarkable response amplification of building frames due to resonance with the surface ground. *Soil Dynamics and Earthquake Engineering* 1998; **17**:211–218.
24. Sextos A, Kappos A, Pitilakis K. Inelastic dynamic analysis of RC bridges accounting for spatial variability of ground motion, site effects and soil-structure interaction phenomena. Part 2: Parametric Analysis. *Earthquake Engineering and Structural Dynamics* 2003; **32**(4):629–652.
25. Stewart JP, Kim S, Bielak J, Dobry R, Power M. Revisions to soil–structure-interaction procedures in NEHRP design provisions. *Earthquake Spectra* 2003; **19**(3):677–696.
26. Kawase H. The cause of the damage belt in Kobe: the basin-edge effect, constructive interference of the direct S-wave with the basin-induced diffracted/Rayleigh waves. *Seismological Research Letters* 1996; **67**(5):25–34.
27. Tokimatsu K, Mizuno H, Kakurai M. Geotechnical aspects of the January 17, 1995 Hyogoken-Nambu earthquake: building damage associated with geotechnical problems. *Soils and Foundations* (Special Issue, January) 1996; 219–234.
28. Gazetas G. *Soil Dynamics and Earthquake Engineering*: *Case Histories* (Symeon editions). Symeon Publishing Co: Athens, Greece, 1996 (in Greek).
29. Fukushima Y, Irikura K, Uetake T, Matsumoto H. Characteristics of observed peak amplitude for strong ground motion from the 1995 Hyogoken Nanbu (Kobe) earthquake. *Bulletin of the Seismological Society of America* 2000; **90**(3):545–565.
30. Mavroeidis GP, Dong G, Papageorgiou AS. Near-fault ground motions, and the response of elastic and inelastic single-degree-of-freedom (SDOF) systems. *Earthquake Engineering and Structural Dynamics* 2004; **33**(9): 1023–1049.
31. Somerville PG, Smith NF, Graves RW, Abrahamson NA. Modification of empirical strong ground motion attenuation relations to include the amplitude and duration effects of rupture directivity. *Seismological Research Letters* 1997; **68**(1):199–222.
32. Ishihara K. Terzaghi Oration: geotechnical aspects of the 1995 Kobe earthquake. *Proceedings of XIVth International Conference on Soil Mechanics and Foundation Engineering*, Hamburg, Germany, 1997; 2047–2073.
33. NEHRP. *Recommended Provisions for Seismic Regulations for New Buildings and other Structures*, Building Seismic Safety Council of National Institute of Building Sciences, Washington, DC, 2003.
34. Matsushima S, Kawase H. 3-D wave propagation analysis in Kobe referring to the 'basin-edge effect'? The effects of surface geology on seismic motion: recent progress and new Horizon on ESG study. *Proceedings of the Second International Symposium*, A.A. Balkema: Rotterdam, 1999; 1377–1384.
35. Kagawa T, Irikura K, Yokoi I. Restoring clipped records of near-field strong ground motion during the 1995 Hyogo-ken Nambu (Kobe), Japan earthquake. *Journal of Natural Disaster Science* 1996; **18**(1):43–57.

36. Schnabel PB, Lysmer J, Seed HB. SHAKE: a computer program for earthquake response analysis of horizontally layered sites. *Report EERC 72-12*, University of California, Berkeley, 1972.
37. Silva W. Soil response to earthquake ground motions. *Report No. RP2556-07*, Electrical Power Research Institute, Palo Alto, CA, 1986.
38. Yoshida I *et al.* Empirical formulas of the SPT blow counts for gravelly soils. *First ISOPT*, 1988; 381–387.
39. Michaelides O, Gazetas G. Non-linear analysis of piles. *Research Report to GGET*, National Technical University, Athens, Greece, 1998 (in Greek).
40. Prakash V, Powell GH, Campbell S. Drain-2DX: base program description and user guide. *UCB/SEMM-93/17*, Department of Civil Engineering, University of California, Berkeley, CA, 1993.
41. Kitrilakis N, Michaelides O, Mylonakis G, Gazetas G. Analysis of pile-soil kinematic interaction under vertical seismic excitation. *Proceedings of the 3rd Greek Conference on Geotechnical Engineering* 1997; 497–503 (in Greek with English Abstract).
42. Syngros C, Mylonakis G, Anastasopoulos I, Gazetas G. The collapse of Fukae (Hanshin Expressway) Bridge, Kobe 1995: contribution of soil–structure interaction, reconstruction and isolation. *Concrete Structures in Seismic Regions*: *FIB 2003 Symposium*, Athens, Greece, 2003; 14.
43. Syngros C, Mylonakis G. Natural period and effective damping of generalized cantilever oscillators on soft soil. *Earthquake Engineering and Structural Dynamics*, under review.
44. Chopra AK. *Dynamics of Structures*: *Theory and Applications to Earthquake Engineering*. Prentice-Hall: Upper Saddle River, NJ, 2001.
45. Veletsos AS. Dynamics of structure-foundation systems. In *Structural & Geotechnical Mechanics*, Hall WJ (ed.). Prentice-Hall: Englewood Cliffs, NJ, 1997; 333–361.
46. Wolf JP. *Seismic Soil–Structure Interaction*. Prentice-Hall: Englewood Cliffs, NJ, 1985.
47. Mylonakis G, Nikolaou S, Gazetas G. Soil-pile-bridge seismic interaction: kinematic and inertial effects. Part I: soft soil. *Earthquake Engineering and Structural Dynamics* 1997; **26**:337–359.
48. Ciampoli M, Pinto PE. Effects of soil–structure interaction on inelastic seismic response of bridge piers. *Journal of Structural Engineering* 1995; **121**(5).
49. JSSMFE. *Geotechnical Investigation Methods* (2nd edn). Japanese Society of Soil Mechanics and Foundation Engineering, 1982.
50. Seed HB, Wong RT, Idriss IM, Tokimatsu K. Moduli and damping factors for dynamic analyses of cohesionless soils. *Journal of Geotechnical Engineering Division* (ASCE) 1986; **112**(GT11):1016–1032.

